Use of fractals to measure anisotropy in point patterns extracted with the DPT of an image

I Fabris-Rotelli[a], A Stein[a,b]

[a] *University of Pretoria, South Africa*
[b] *University of Twente, The Netherlands*

Abstract

Images are particular and well–known instances of spatial big data. Typically spatial data are scale specific and in this paper, we propose mechanisms to effectively address issues of scale in the analysis of images. We focus on spatial data extracted from images using the Discrete Pulse Transform (DPT). The DPT extracts discrete pulses from images at multiple scales that are recognisable as connected components. Traditionally, fractals are used for this purpose, but they fall short as the process underlying fractality is usually either absent or poorly understood. This paper investigates the Ht-index (head/tail break) as an alternative, merging ideas from image analysis and spatial statistics. More specifically, we use the Ht-index for the analysis of anisotropic point patterns that are obtained from applying the DPT. We propose a multi-level Ht-index decomposition in this regard. This is the first mechanism for the DPT enabling an informed partition of the scale-space. The results show that the Ht-index is well suited to identify the anisotropic structure location within specific scales and thereby substantially reduces computational costs. We conclude that the use of the Ht-index is promising and is well-suited for the further analysis of spatial big data.

Keywords: Discrete Pulse Transform, fractal, Ht-index, anisotropy, spatial point pattern, texture image

1. Introduction

Big spatial data show computational complications, as they are more intense than non-spatial big data. The analysis in such a case still requires attention. Here we focus on spatial data extracted from images by using the Discrete Pulse Transform (DPT) [1]. The DPT extracts discrete pulses, recognisable as connected components, from images at multiple scales. The scale is measured as the number of pixels. Scaling is referred to in a geographical sense as a universal form or pattern occurring across scales [2]. These DPT pulses at various scales characterise the texture of an image and can be effectively spatially modelled as point patterns, as shown in [1]. The size of the resulting point pattern presents big spatial data having in the 100 000's points for a single band image. Texture knowledge is useful for remote sensing classification applications, for example, but further adds complexity to big

spatial data due to the presence of multiple scales, resolution and multivariate data. We are specifically interested here in determining the anisotropy of such a point process with the view of picking up directionality in an image for texture analysis. Al-Saidi and Abdul-Wahed [3] define a image texture as "a structure that preserves some statistical properties in the color or brightness distribution and repeatedly makes patterns". Fazel-Rezai and Kinsner [4] state that texture provides essential structure information of an image and Roux et al [5] comment that self-similar processes with anisotropy model image texture processes well. In the past, the fractal dimension has been investigated in image analysis, specifically texture analysis. The theoretical development has increased as computing grows [6, 7, 8, 9, 10, 11, 12, 13, 14, 15]. It has been used in remote sensing [3, 16, 17, 18, 19, 20, 21, 22], image inpainting [23, 24], image matching with texture [25], denoising [26, 27], restoration [28], segmentation [7], compression [29, 30], shape classification and segmentation [8, 31], interpolation [32], classification [33], superresolution [34], medical imaging [35, 36, 37, 38] and specifically in texture analysis [39, 40, 4]. Wavelet based techniques are also widely used and are powerful in image processing techniques. They have been used in directional texture analysis in [41, 42, 43, 44, 45, 5]. The DPT provides an alternative multiscale method, which has a number of advantages. It provides an already discrete approach to extracting multiscale information from images. Further, it has strong mathematical properties such as the use of non-linear idempotent operators with a semi-group structure, edge-preservation (non-blurring) and structure consistency with a perfect reconstruction obtained via a simple sum. The novelty of this paper is that we merge the idea of directional image analysis with spatial analysis of point patterns, providing also the first method to extract important scales of the scale-space built by the DPT.

We now turn to identifying the fractal structure of the DPT. A set or pattern is said to be fractal if there are far more small pattern elements than larger or, similarly, the scaling pattern of this abundant small pattern elements compared to large occurs numerous times [46]. Fractal geometry [47, 48] provides a geometry for rough and irregular forms, including a quantitative value known as the fractal dimension. The fractal dimension, however, requires strict self-similarity through a power law that is seldom present in data with heavier tails. To overcome this problem, in this paper we investigate the Ht-index as an alternative fractal measure in images, merging ideas from image analysis and spatial statistics. The Ht-index (head/tails break) [49] provides an effective method to visualise the hierarchy of a complex system. It measures the fractal nature of geographical data, as an alternative to the global natural breaks classification [50], which minimizes intraclass variance but is unable to capture scaling structure. The Ht-index allows for any functional form and captures geostatistical data more appropriately [51]. It is defined as the number of repetitions for which the following is observed: the mean scale thresholds the data so that the majority ($> 50\%$) of data values fall to the left of the mean scale. The subsequent repetition is conducting on only the data in the smaller tail. Larger complexity

is visible with more repetitions measured. The Ht-index captures the idea of having many more small elements than large elements. It has been applied to city sizes, streets, population densities on lattice data, night light imagery pixel values, terrain surface DEM values and the evaluation of natural cities [2, 52, 53], to name a few areas.

A DPT pattern can be seen as a collection of points, where the points all have a fractal shape. We note for instance that small point patterns are more naturally isotropic and stationary [54]. Hence, stationarity and isotropy of the DPT should be checked carefully. This can be complicated in the light of the the big data nature of the DPT. Simply sampling the point pattern to reduce size is not effective. Ratcliffe [55] shows that a 85% sample is needed to maintain the structure of a point pattern. This size sample does not alleviate the big data aspect. We thus make use of the Ht-index as a fractal measure for spatial data from images to extract the true texture structure in a knowledgeable way. Li et al [46] state that the next step using the Ht-index is to develop an understanding of the fractal structure. We do so here for point patterns extracted from texture images using the DPT. Jiang [2] states that "scaling, if visualised properly using head/tail breaks can evoke a sense of beauty". We decompose an image to demonstrate this visualisation.

The objective of this paper is to use the Ht-index for the analysis of point patterns that are obtained from applying the DPT on anisotropic images. The paper is structured as follows. Section 2 considers images in the context of big spatial data. Section 3 describes the extraction of a texture point pattern using the DPT, the employment of the Ht-index to this point pattern and then anisotropic analysis. Section 4 applies the ideas to a texture image from the Brodatz texture database[1]. Section 5 discusses the results and Section 6 concludes and suggests further avenues.

2. Images as big spatial data

Big spatial data (BSD) have an even larger impact computationally than traditional big data. In particular, spatial autocorrelation [56], non-stationarity and anisotropy have to be considered. These properties are defined in terms of distances between pairs of points, hence BSD are more computationally intensive than non-spatial big data [57] and have further challenges as discussed in [58]. There have been a number of books on BSD recently published [59, 60, 61]. A number of discussions on BSD and avenues to investigate can be found in [46, 62, 63, 56]. A shift to data-driven research and non-iterative algorithms, the need for improved spatial indexing, improved visualisation informed by human cognition and quality assurance are highlighted.

Remote sensing image analysis has emerged in the past decades and big data for this analysis has been explosive due to location-aware software. With the volume of data increasing with varying format

[1] http://www.ux.uis.no/ tranden/brodatz.html

the big data aspect frequently starts discussion. Big spatial data provide valuable information for more informative decision making. It has a huge potential in society such as water management, agriculture, transportation and public health [64, 46]. Smarter computing has been investigated to deal with BSD such as cluster computing [65], Hadoop-GIS for spatial querying [66], Hadoop and MapReduce [67, 68], development of a spatial cumulative sum algorithm [69], GPU usage [70], cloud computing [71] and Java and Apache Spark [72].

3. Methodology

The DPT is a nonlinear multiscale decomposition of an image obtained through recursive application of the operators L_n and U_n [73]. The Discrete Pulse Transform (DPT) is obtained via the sequential application of the LULU operators L_n and U_n, $n = 1, 2, .., N$ where N is the total number of pixels in the image. They are defined for $f \in \mathcal{A}(\mathbb{Z}^2)$, a vector lattice, and $n \in \mathbb{N}$, as

$$\begin{aligned} L_n(f)(x) &= \max_{V \in \mathcal{N}_n(x)} \min_{y \in V} f(y), \ x \in \mathbb{Z}^2 \ , \\ U_n(f)(x) &= \min_{V \in \mathcal{N}_n(x)} \max_{y \in V} f(y), \ x \in \mathbb{Z}^2 \ , \end{aligned}$$

where $\mathcal{N}_n(x) = \{V \in \mathcal{C} : x \in V, \text{card}(V) = n + 1\}$ and $\mathcal{C}$ is a connection (see [1] for details not repeated here). The well-known concepts of 4- and 8-connectivity within pixel lattices are examples of mathematical connections. We make use of 4-connectivity for the DPT here, however the LULU operators are defined on any chosen connection satisfying the required connectivity properties.

The DPT is obtained via iterative application of the operators L_n, U_n with n increasing from 1 to N, decomposing the image into a number of pulses $\phi_{ns}, s = 1, ..., \gamma(n)$, where n is the scale (number of pixels in the connected component) and $s = 1, ..., \gamma(n)$ the number of pulses at scale n, using the operations $P_n = L_n \circ U_n$ or $P_n = U_n \circ L_n$ and then $Q_n = P_n \circ P_{n-1} \circ ... \circ P_1$. The number of pulses at each scale n varies and is represented as $\gamma(n)$ to clarify this. A pulse ϕ_{ns} is defined on a connected set $V \subset \mathbb{Z}^2$ if it has value c (some constant) for $x \in V$ and value 0 otherwise. At each iteration the portions of the image which are filtered out by the application of P_n, $n = 1, 2, ..., N$ i.e. $(I - P_n)(f) = D_n(f)$, are retained until we obtain $Q_N(f)$, a constant function, where I is the identity operator. The function f is then decomposed as the DPT of f:

$$f = \sum_{n=1}^{N} D_n(f) = \sum_{n=1}^{N} \sum_{s=1}^{\gamma(n)} \phi_{ns}$$

into pulses ϕ_{ns} [1]. The maximum scale is N which is the total number of pixels in the image being considered. Further details are shown in [1] and [73]. This image decomposition provides us with information about the structure content of the image at all scales from $n = 1$ up to N.

We provide a short example to illustrate. Consider a tiny image

$$f = \begin{bmatrix} 2 & 1 & 3 \\ 5 & 4 & 3 \end{bmatrix}.$$

The DPT proceeds as follows, sequentially removing local maximum and minimum sets,

$$\begin{aligned} L_1(f) &= \begin{bmatrix} 2 & 1 & 3 \\ 4 & 4 & 3 \end{bmatrix} \\ U_1L_1(f) &= \begin{bmatrix} 2 & 2 & 3 \\ 4 & 4 & 3 \end{bmatrix} \\ L_2U_1L_1(f) &= \begin{bmatrix} 2 & 2 & 3 \\ 3 & 3 & 3 \end{bmatrix} \\ U_2L_2U_1L_1(f) &= \begin{bmatrix} 3 & 3 & 3 \\ 3 & 3 & 3 \end{bmatrix} \end{aligned}$$

so that f is decomposed as the connected portions removed at each filtering

$$f = \begin{bmatrix} 0 & 0 & 0 \\ 1 & 0 & 0 \end{bmatrix} + \begin{bmatrix} 0 & -1 & 0 \\ 0 & 0 & 0 \end{bmatrix} + \begin{bmatrix} 0 & 0 & 0 \\ 1 & 1 & 0 \end{bmatrix} + \begin{bmatrix} -1 & -1 & 0 \\ 0 & 0 & 0 \end{bmatrix} + \begin{bmatrix} 3 & 3 & 3 \\ 3 & 3 & 3 \end{bmatrix}.$$

As is seen in the example, due to the multiscale nature each pixel can belong to multiple pulses at different scales.

We focus on the pulses as spatial units and apply the Ht-index to them. The number of pulses is huge presenting BSD. The use of the Ht-index on this type of data provides informative fractal levels. The Ht-index is defined as one plus the recurring times for which there are more small structures than large, that is, it equals h if this recurs $h-1$ times [52]. The procedure for calculation of the Ht-index is as a first step to determine the mean scale of all the structures. The number of structures smaller than this mean, n_{less}, and the number of structures larger than this mean, n_{more}, are calculated. If $n_{less} > n_{more}$, the second step is to repeat this process. The mean of the tail (the scales to the right of the first mean) is calculated and again the number of structures less and more than this mean in the tail are counted. This is repeated until the $n_{less} \leq n_{more}$. The Ht-index is the number of recursions plus one, representing the number of scale interval divisions.

Consider for example, a DPT decomposition consisting of 8 pulses with sizes 1, 1, 1, 1, 2, 2, 6, 7 respectively. The size of the pulse is the number of non-zero entries in the array, referred to as the scale. The mean of these scales is 2.625, with the values 1, 1, 1, 1, 2, 2 being less than this mean and the values 6 and 7 being larger than this mean, so that 75% are less than the mean and 25% larger than the mean. This shows that there is a majority (more than 50%) of smaller scales. The values

smaller than the mean are then discarded and this process repeated for the scale values 6 and 7. The mean is then 6.5 for which exactly 50% of the values are smaller and 50% are larger. The process thus stops and Ht-index is determined as 2.

We propose here to further calculate the Ht-index of the pulses at each majority smaller scale interval until no further majority smaller scale intervals are present, thereby constructing a multi-level Ht-index for BSD that is specifically applicable to textures in images. For the example above this means we calculate the Ht-index for the values 1, 1, 1, 1, 2, 2 obtaining the mean $1.\dot{3}$. Then $66.\dot{6}\%$ of the values are less than this mean (the values 1, 1, 1, 1) and $33.\dot{3}\%$ are larger (the values 2, 2). The process is repeated for the tail values 2, 2. The mean is 2 so there is no majority percentage and the process stops with h obtained as 2. The multiscale Ht-index is then represented as $h = 2$ at level 1 and $h = 2$ at level 2.

We now turn to point patterns, denoted by $x = \{x_1, ..., x_n\}$ and position the DPT decomposition as such. Point patterns are well described elsewhere [74]. An important property of point patterns, which is relevant in our study, is their invariance under rotations. If the distribution of a point pattern is invariant under rotations about the origin, then it is called isotropic, otherwise it is called anisotropic. Anisotropy in point processes may occur as either geometric, which is equivalent to a linear transformation of a stationary and isotropic process, or zonal if it shows increased intensity along directed lines [54]. Anisotropy has been studied in some detail. Directional distributions are derived in [75], wavelet analysis has been presented in [76, 77], tests on the angular directions have been developed in [78, 79, 74], ellipsoids are fitted to Fry plots to test for geometric isotropy in [80] and the second-order intensity function has been used in [81], to list some. Here we focus on multi-level fractal visualisation of rose diagrams for BSD, extracted from multiscale image decompositions.

The point pattern extracted from the DPT is determined as follows, as in [1]. Consider a point process $Z(x)$ on $\mathbb{Z}^2$. The spatial window is extent of the image, for example, an $N \times M$ image will be modelled on a continuous rectangular widow of size $[0, N] \times [0, M]$. The process $Z(x)$ takes on 1 if there is a pixel belonging to a pulse at position x and 0 otherwise, where position x is the center of the pixel on the continuous domain. This is illustrated in Figure 1. The approach of a regular lattice is also to be considered but adds no additional modelling advantages[2].

4. Application

Figure 2 shows image D15 of the Brodatz texture database, a linear texture. It is used here due to its obvious upward directionality of texture. In addition, it is has a stationary structure in

[2] Spatial lattice data typically consists of polygonal areas. When these polygons represent the pixel areas the lattice is referred to as regular.

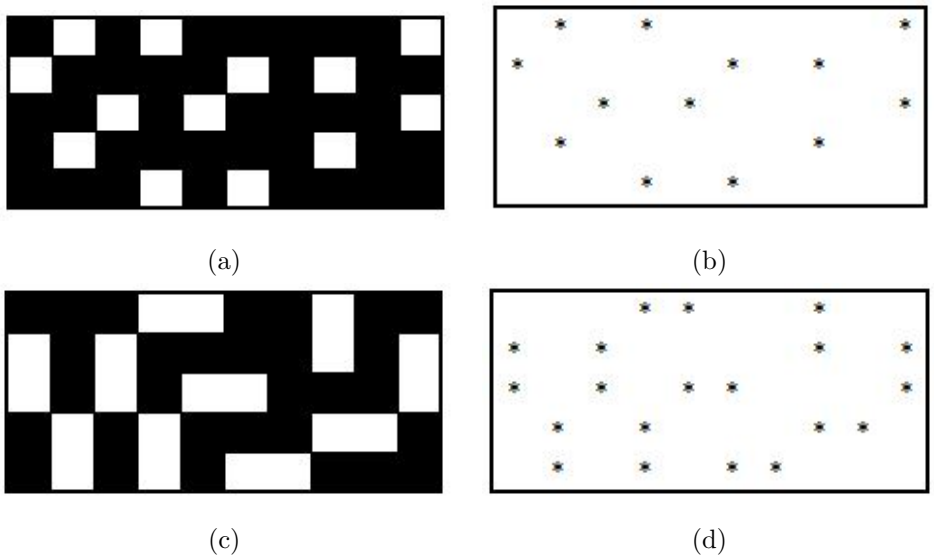

Figure 1: (a) Sample of pixels at scale 1 (black indicates background, white indicates foreground); (b) Extracted point pattern for (a); (c) Sample of pixels at scale 2; (d) Extracted point pattern for (c).

that the intensity does not drastically vary over the domain. Non-stationarity would detract from the investigation here on anisotropy. In Figure 3 the number of pulses ϕ_{ns} of the DPT $f = \sum_{n=1}^{N} \sum_{s=1}^{\gamma(n)} \phi_{ns}$ is plotted. The total number of pulses equals 139131 for this texture. The number of pulses $\gamma(n)$ for small n is large and when plotted for all n the plotted values are so close to the x-axis, not discernible as the values decrease from very large to very small at a large pace. In Figure 3 only scales 1 to 100 are thus shown. The number of pulses $\gamma(n)$ for $n = 1$ to 100 is shown in Figure 3(a), whereas Figure 3(b) shows the logarithm of both axes, the Richardson plot of Mandelbrot [47, 48]. This plot is indicative of self-similarity: a perfect straight line shows strict self-similarity and the slope of the line is the fractal dimension. Spatial data are known to not show strict self-similarity, but rather statistical self-similarity with the points around the line rather than on it [51]. This requires a functional form other than a power function, for example the use of the Ht-index.

We start by looking at scales $n = 1$ to 114. The reason for choosing 114 will become clear shortly. The point pattern extracted when using pulses at scales $n = 1$ to 114 results in 243969 points over a continuous spatial domain $[0, 640] \times [0, 640]$ (resulting from the image of 640×640 pixels). The

Figure 2: Image D15 from the Brodatz texture database

associated image in shown in Figure 4(a)[3]. This is a partial reconstruction obtained as

$$f_{rec} = \sum_{n=n_1}^{n_2} \sum_{s=1}^{\gamma(n)} \phi_{ns} \tag{1}$$

for scale interval $[n_1, n_2]$. Simple sampling will not be effective for such a large pattern. Decomposition of the point pattern into meaningful scale partitions for sub-analysis proves valuable. We propose the use of the Ht-index in this endeavour.

Figure 5 graphically illustrates the partition of the large point pattern of image D15 using the Ht-index. At first application the number of pulses at each scale n results in recursively calculated mean scales 114, 940, 4886, 17836, 49140 and 107423 which have majority of pulses, shown in percentages to the left of the mean in the figure, respectively. The majority percentages are 89%, 86%, 81%, 78%, 70% and 55%. A high value for h implies a larger complexity. This gives a Ht-index of $h = 7$, indicating a complex structure. The $h = 7$ implies that 6 means were calculated resulting in 7 scale intervals. Note the choice of the value of 114 should now be clear as 114 is the first mean calculated. Figure 4 shows the reconstructed images for each of these scale intervals. We propose to further implement the Ht-index within each of these majority intervals as the size of the point patterns in these 6 intervals is still large, see Table 1. Implementing the Ht-index on the pulses over scales $[1, 114]$ results in means 14,

[3] Note: These grey levels are chosen by default for visual purposes when reconstructing the images with less of the original information in order to maximally distinguish between the different areas (pulses) in the reconstruction. They are simply visual grey levels scaled for maximum differentiation.

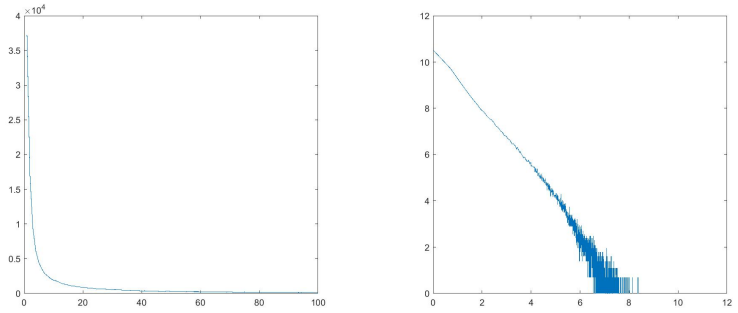

(a) Number of pulses for $n = 1$ to 100

(b) Richardson plot: $\log(n)$ vs $\log(\gamma(n))$

Figure 3: Number of pulses extracted using the DPT for image D15 of Figure 2

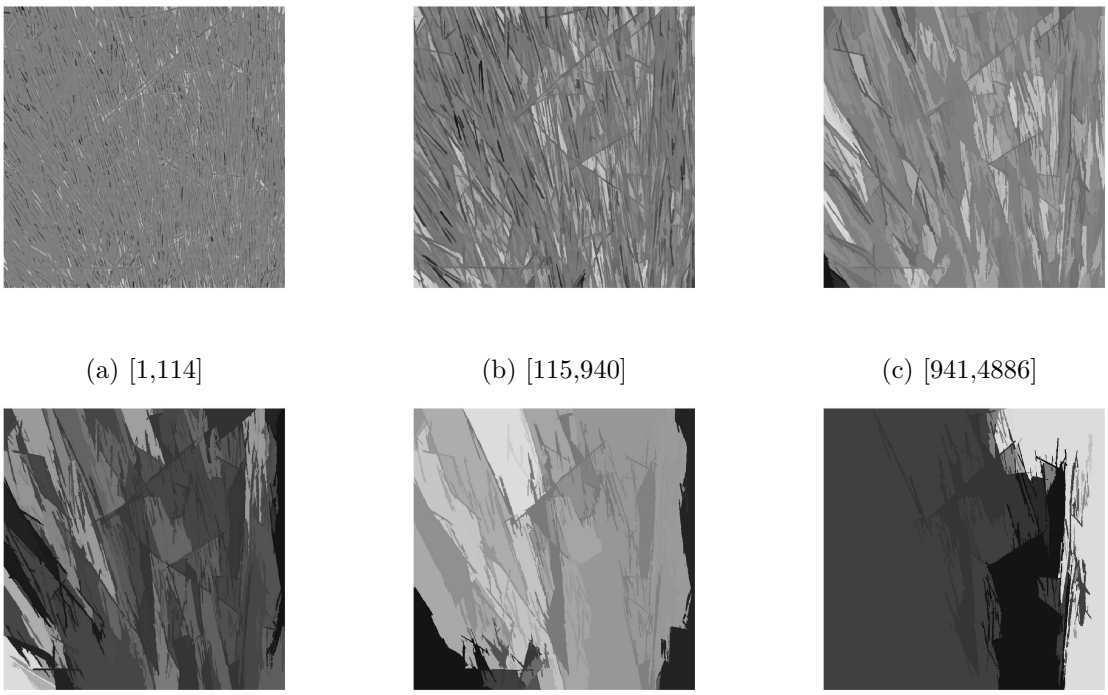

(a) [1,114]

(b) [115,940]

(c) [941,4886]

(d) [4887, 17836]

(e) [17836,49140]

(f) [49141, 107423]

Figure 4: Partial DPT reconstructions for the scale intervals of level 1 of the multi-level Ht-index using equation (1)

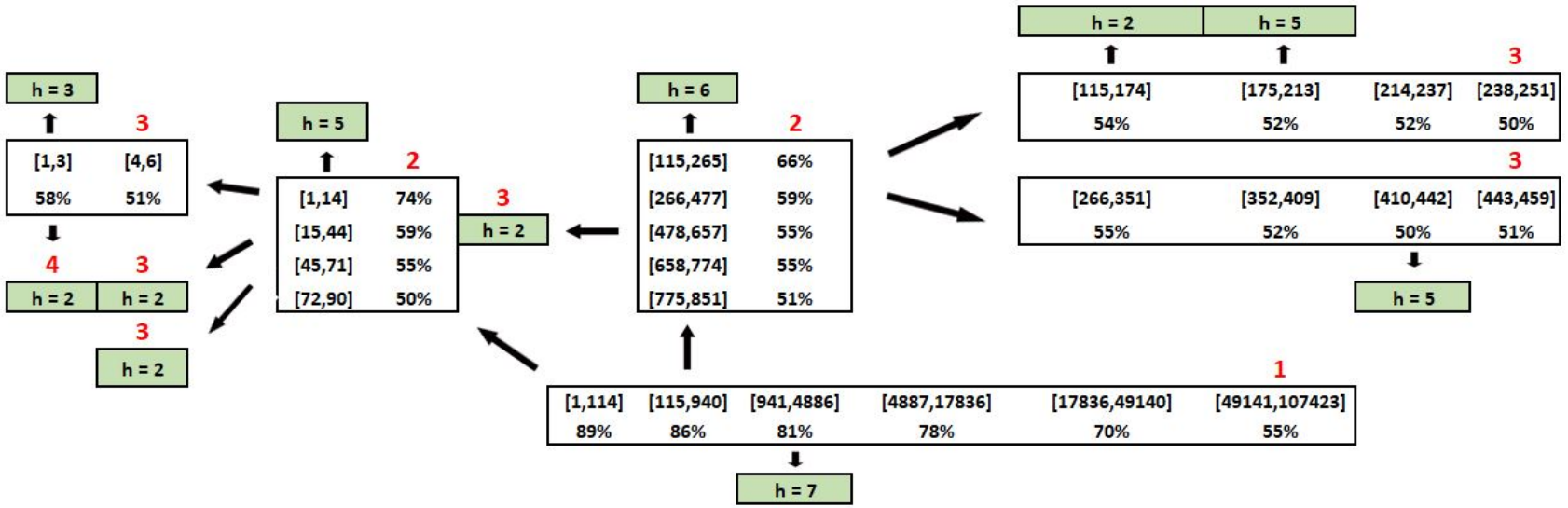

Figure 5: Multi-level Ht-index for Brodatz image D15. Scale intervals are group and their Ht-index, h, shown for each group. Levels 1,2,3 and 4 indicate the level of the Ht-index i.e. at what recursion it was calculated, creating a hierarchical structure.

44, 71 and 90 with the majority of pulses to the left of the mean, resulting in $h = 5$. The percentages are also shown, as before, in Figure 5. This is repeated for scales $[115, 940]$ which results in means 265, 477, 657, 774 and 851, with $h = 6$. The remaining 4 intervals corresponding to means 4886, 17836, 49140 and 107423 show no self-similarity, that is, no majority to the left. This second application of the Ht-index within the first scale intervals of $h = 7$ is labelled as level 2 in Figure 5. Level 3 is the Ht-index applied to the level 2 intervals. Interval $[1, 14]$ has means 3 and 6, with $h = 3$. Interval $[15, 44]$ has $h = 2$, as does interval $[45, 71]$. Interval $[115, 265]$ has means 174, 213, 237 and 251, with $h = 5$. Interval $[266, 477]$ has means 351, 409, 442 and 459, also with $h = 5$. Interval $[478, 657]$ has $h = 2$. Level 4 is only present for intervals $[1, 3]$ and $[115, 174]$ both with $h = 2$. We only consider scale intervals for $h > 2$ to extract maximum complexity. In Figure 5 those intervals without an Ht-index show no fractal structure, that is there is no majority pulses to the left of the mean. A full fractal decomposition of the DPT scale-space has been achieved. This is the first mechanism for the DPT enabling an informed partition by scale of the scale-space.

Figures 8 and 9 show the kernel density fitted intensities of each scale interval for levels 1 to 3. The intensities for scale [1,114] on level 1, [1,14] on level 2 and [1,3] on level 3, the smallest scales at each level, show a strong trend and they capture the complexity of the texture. The associated rose diagrams are shown in the same figure[4]. The vertical anisotropy is captured in the scales [1,114], [1,14] and [1,3] and more so at level 3 than at level 1. The image under consideration has mostly vertical directionality but the left of the image can be seen to have some directionality to the North-West. The rose diagrams pick this up in the point pattern extracted from the DPT. This indicates the ability of a multi-level Ht-index decomposition for capturing the scales contributing most significantly to the texture structure. These three scale intervals also have the largest point pattern size as seen in Table 1. The sizes are 243969, 133470 and 74251 respectively. This Ht-index decomposition thus provides an informative way to reduce the data size to the 74251 of scales [1, 3], which captures the anisotropy in a clear manner. The DPT is computationally heavy due to not being parallelisable when implemented [82]. It however provides useful information for the scale information in an image enabling many image processing improved results, see [83] for example. The size of the point pattern extracted from the pulses as described earlier is very large resulting in many spatial point pattern analysis tools not being viable for example a Fry plot and model fitting as well as diagnostics [1]. Having a method to thus reduce the number of pulses of the DPT and the extracted point pattern means that extracting the

[4]The rose diagram implemented here does not use the point pair distribution. The implementation used is that of *S*patstat in *R* and uses the nearest neighbour angles only. It does not thus repeat in the opposite direction producing symmetry. Of course one could take the n^{th} nearest neighbours as an alternative, say up to $n = 10$ (with n chosen wisely). This was investigated and only adds more smoothing to the rose diagram.

anisotropy information is at a more manageable data size. Thus the big data and computational issues have been alleviated by analysing the appropriate scales of the DPT. This approach also provides avenues for future techniques employing the DPT pulses when appropriate scale choices should be made. It allows for data specific scale choice instead of ad hoc decisions.

Level 1		**Level 2**		**Level 3**	
[1, 114]	243969	[1, 14]	133470	[1, 3]	74251
[115, 940]	100	[15, 44]	15	[4, 6]	4
		[45, 71]	44	[115, 174]	100
		[72, 90]	73	[175, 213]	100
		[115, 265]	100	[214, 237]	195
		[266, 477]	213	[238, 351]	231
		[478, 657]	477	[352, 409]	353
		[658, 774]	610	[410, 442]	413
		[775, 851]	759	[443, 459]	376

Table 1: Point pattern sizes for each scale interval at levels 1 - 3

The method of using the DPT to extract pulses from an image and then representing the pulses in a spatial point pattern means that the anisotropy detected is that of the original image process. The origin of the image content is of course continuous from the underlying process, captured into a discretised image. With higher resolution the captured image more accurately represents the true scene. This should always be considered in image analysis as an accuracy level and what results are referred back to the true scene. The image process is presented in an alternative form through a point pattern but the same information is captured. The idea of using the Ht-index is to determine the scales from the multiscale DPT decomposition in which the anisotropy is present. Most of the scale levels are details (at fine scales) or background shading (at coarse scales). We thus harness this multiscale representation using the Ht-index and determine the scales which carry the anisotropy information of the process.

The results on the anisotropic image show that the Ht-index provides useful breaks for placing different scale intervals into hierarchical levels for optimised spatial analysis of BSD. The anisotropy is captured at other scale intervals as well (see Figures 8 and 9) but is not as strong. This provides a novel data-driven technique to model using the correct scales of the DPT that has not been applied to images decomposed in a multiscale manner before. Further investigation could delve deeper into the philosophical components of texture such as investigated in [84].

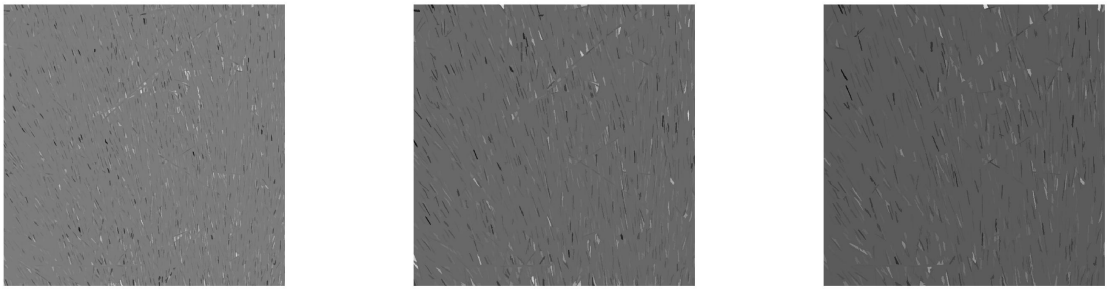

(a) [15,43] (b) [44,71] (c) [72,90]

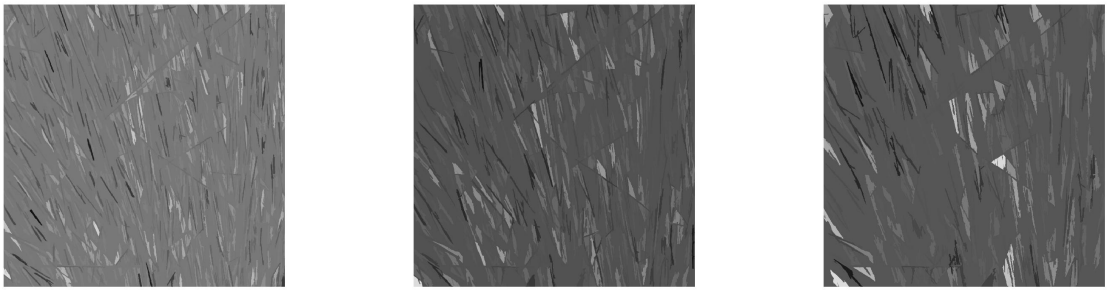

(d) [115,265] (e) [266,477] (f) [478,657]

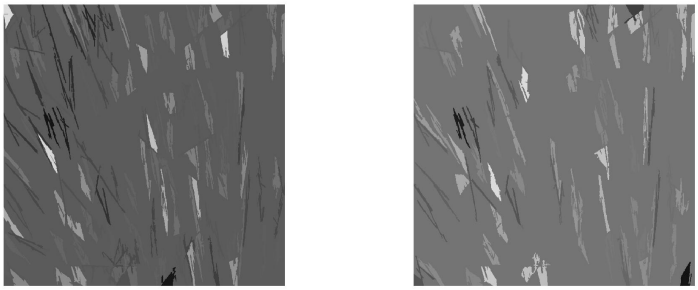

(g) [658,774] (h) [775,851]

Figure 6: Partial DPT reconstructions for the scale intervals of level 2 of the multi-level Ht-index

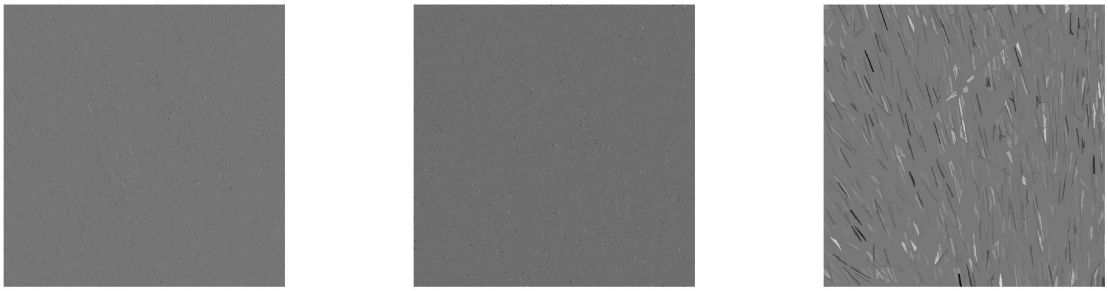

(a) [1,3] (b) [4,6] (c) [115,174]

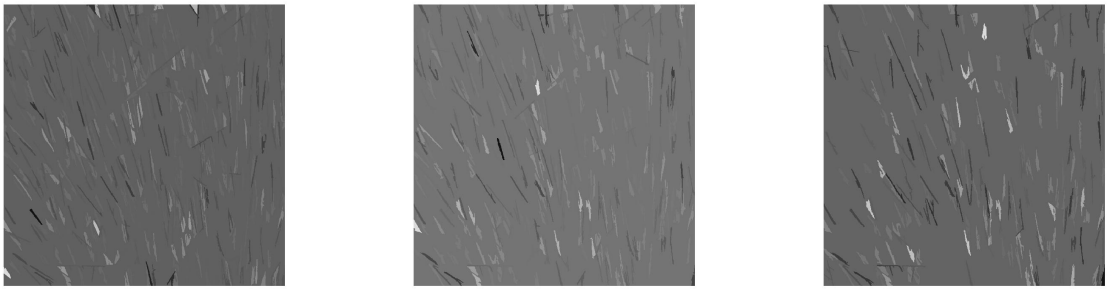

(d) [175,213] (e) [214,237] (f) [238,351]

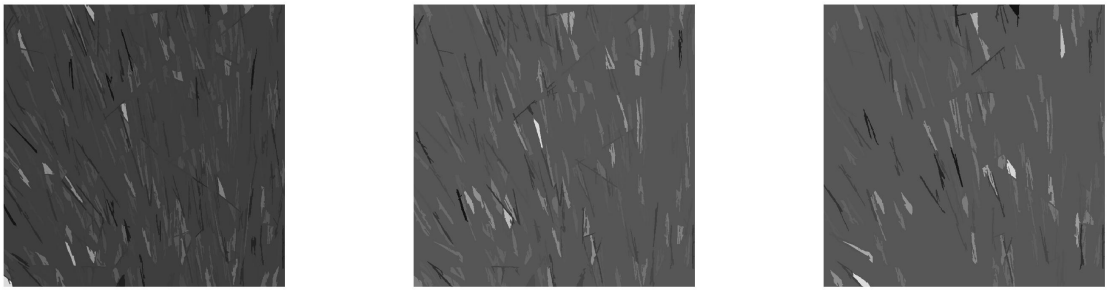

(g) [266,351] (h) [352,409] (i) [410,442]

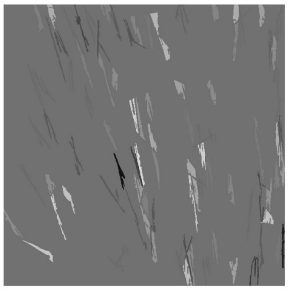

(j) [443, 459]

Figure 7: Partial DPT reconstructions for the scale intervals of level 3 of the multi-level Ht-index

LEVEL 1

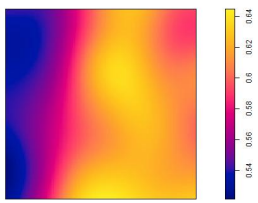

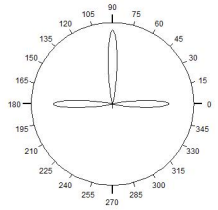

(a) [1,114]

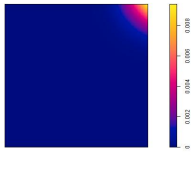

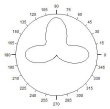

(b) [115,940]

LEVEL 2

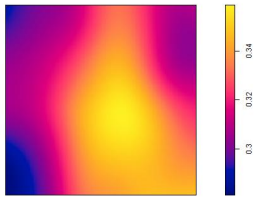

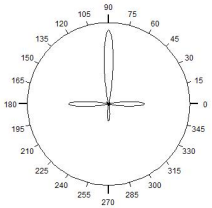

(c) [1, 14]

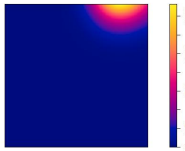

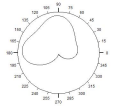

(d) [15, 44]

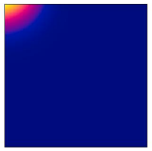

(e) [45, 71]

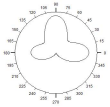

(f) [72, 90]

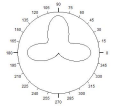

(g) [115, 265]

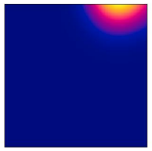

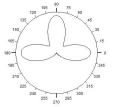

(h) [266,477]

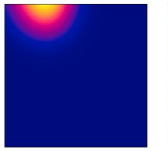

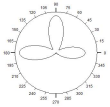

(i) [478, 657]

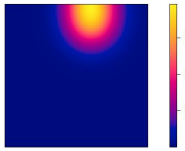

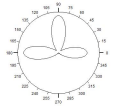

(j) [658, 774]

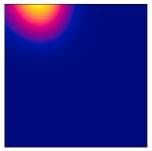

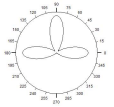

(k) [775, 851]

Figure 8: Kernel density plots of the intensities and rose diagrams for the associated point patterns at each intervals for levels 1 - 2. Plots (a) and (c) are shown larger for detail.

LEVEL 3

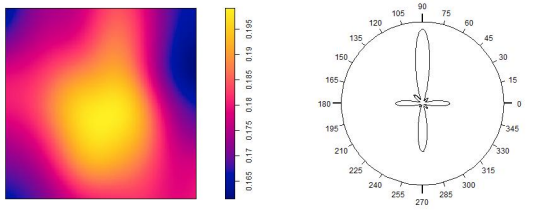

(a) [1, 3]

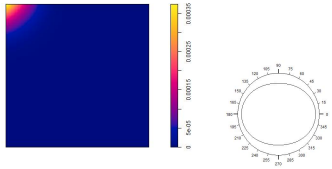

(b) [4, 6]

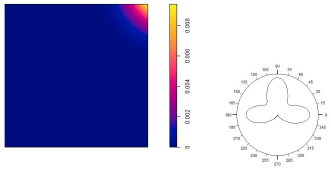

(c) [115, 174]

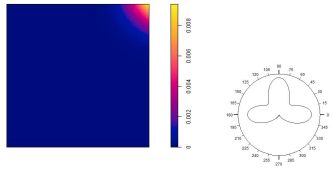

(d) [175, 213]

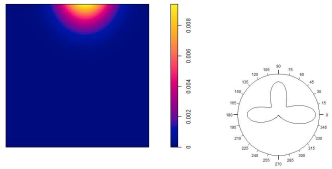

(e) [214, 237]

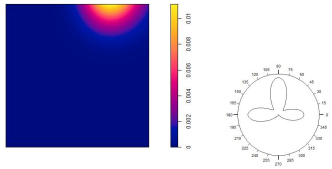

(f) [238, 251]

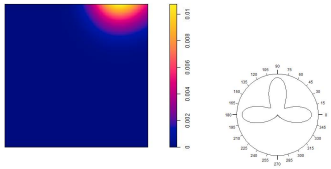

(g) [266, 351]

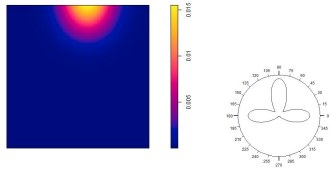

(h) [352, 409]

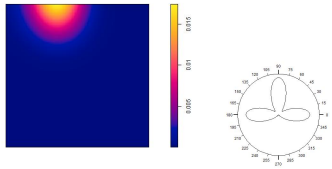

(i) [410, 442]

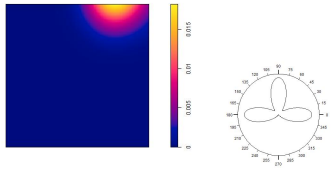

(j) [443, 459]

Figure 9: Kernel density plots of the intensities and rose diagrams for the associated point patterns at each intervals for levels 3. Plot (a) is shown larger for details.

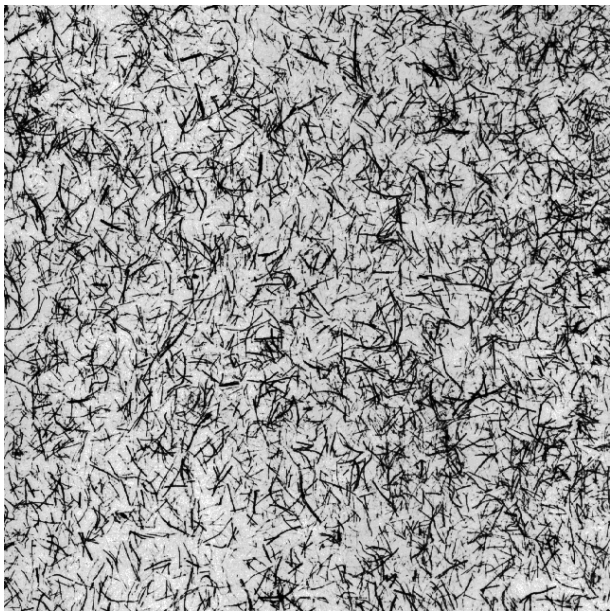

Figure 10: Image D110 from the Brodatz texture database

The intensities shown in Figures 8 and 9 also pick up the heterogeneity of the texture. The three intervals [1,114], [1,14] and [1,3] are those scale intervals containing the heterogeneity. The other intervals show only isolated intensities, not indicative of a pattern. This multi-level Ht-index thus also provides a mechanism for characterising heterogeneity.

To provide a counter example, what we deemed the most isotropic image from the Brodatz texture database was also investigated, image D110, seen in Figure 10. The Ht-index multiscale method proposed nonetheless still picks up the anisotropy in this image as well. This is due to the natural anisotropic nature of all images. In [85, Section 5.7] the anisotropy of natural images is confirmed through measurement of image statistics. This is obvious once one thinks about it. A natural image must have rotational variation to express its content, even with repetition present. Thus, a true isotropic image can only be simulated.

5. Discussion

This paper focused on anisotropy, whereas, more complex spatial modelling can also be investigated, for example fitting cluster models at each level enabling parallelisation of spatial data. In addition, multiple bands and spatio-temporal data should also be investigated for a fractal decomposition.

There have been two suggested extensions to Jiang's Ht-index: the CRG-index [86] and the ratio of areas (RA) [87]. The CRG index is said to be a more sensitive Ht-index using adaptive breaks, and the RA captures more heterogeneity. The implications of these to the DPT may yield further insights

in future research.

Image D15 of the Brodatz texture database was chosen as it does not exhibit any obvious non-stationarity. Future analysis should determine if the multi-level Ht-index proposed can pick up non-stationarity. The Second Law of Geography states that geographic events are more likely to occur in some locations than at other locations, that is, spatial non-stationarity. There is also not something like an average location [88, 89]. Non-stationarity should be determined for data being considered. Interestingly, the Ht-index has been used to capture non-stationarity in spatial data as well as [90] and was able to formulate non-stationarity as a scaling law [91]. Modelling of this specific texture using a line process should also provide interesting results and we plan to do this in a future study.

The presence of noise in an image should not be disregarded. Noise (if additive and not multiplicative) will simply add more small structures, thus increasing the Ht-index. Any anisotropy identification in images should involve a noise removal step, as do most image processing tasks. An interesting phenomenon may occur in the presence of multiplicative noise, where the noise may be part of the signal as in radar images. But here again, this more structural form of noise should be dealt with before testing for anisotropy. A simulation study on various noise types added will yield interesting results in the future.

6. Conclusion

This study showed that the Ht-index is an efficient and effective visualisation tool to analyse anisotropic point patterns obtained from images as a specific form of spatial big data. We have shown this for a point pattern extracted from a texture image process, using the extracted fractal levels for anisotropy analysis. Applying the Ht-index at multiple levels provides useful breaks for optimised spatial analysis. We found that the multi-level Ht-index is an important method for anisotropy analysis. It allowed us to deal with spatial big data in a knowledgeable, data-driven way, and it captures the inherent hierarchy of spatial features. We foresee that this will be significant as well for use in statistical mapping and cognitive mapping. In future the simulation of directional self-similar images, such as in [5], will provide an extension to this study. In addition, a study of simulated isotropic and anisotropic images, similar to the approach in [92], will reveal further insight to this proposed new multiscale Ht-index.

Acknowledgements

Funding from the University of Pretoria's Vice-Principal Congress Funding and Statomet from the Department of Statistics, University of Pretoria is acknowledged for this research.

References

[1] I. Fabris-Rotelli, A. Stein, Inhomogeneous spatial modelling of DPT pulses for marine images, Spatial Statistics 28 (2018) 257–270.

[2] B. Jiang, D. Sui, A new kind of beauty out of the underlying scaling of geographic space, The Professional Geographer 66 (2014) 676–686.

[3] N. Al-Saidi, H. Abdul-Wahed, Classification of remote sensing images via fractal discriptores, in: 2018 International Conference on Advance of Sustainable Engineering and its Application (ICASEA), IEEE, 2018, pp. 99–104.

[4] R. Fazel-Rezai, W. Kinsner, Texture analysis and segmentation of images using fractals, in: Engineering Solutions for the Next Millennium. 1999 IEEE Canadian Conference on Electrical and Computer Engineering (Cat. No. 99TH8411), volume 2, IEEE, 1999, pp. 786–791.

[5] S. Roux, M. Clausel, B. Vedel, S. Jaffard, P. Abry, Self-similar anisotropic texture analysis: the hyperbolic wavelet transform contribution, IEEE Transactions on Image Processing 22 (2013) 4353–4363.

[6] S. Chen, J. Keller, R. Crownover, On the calculation of fractal features from images, IEEE Transactions on Pattern Analysis and Machine Intelligence 15 (1993) 1087–1090.

[7] T. Ida, Y. Sambonsugi, Image segmentation and contour detection using fractal coding, IEEE Transactions on Circuits and Systems for Video Technology 8 (1998) 968–975.

[8] S. Kisan, S. Mishra, D. Mishra, A novel method to estimate fractal dimension of color images, in: 2016 11th International Conference on Industrial and Information Systems (ICIIS), IEEE, 2016, pp. 692–697.

[9] A. Lam, Q. Li, Fractal analysis and multifractal spectra for the images, in: 2010 International Symposium on Computer, Communication, Control and Automation (3CA), volume 2, IEEE, 2010, pp. 530–533.

[10] S. Liu, An improved differential box-counting approach to compute fractal dimension of gray-level image, in: 2008 International Symposium on Information Science and Engineering, volume 1, IEEE, 2008, pp. 303–306.

[11] G. Melnikov, The fractal method of the image coding, in: 2007 Siberian Conference on Control and Communications, IEEE, 2007, pp. 153–157.

[12] J. Rigaut, D. Schoevaert-Brossault, A. Downs, G. Landini, Asymptotic fractals in the context of grey-scale images., Journal of Microscopy 189 (1998) 57–63.

[13] D. Rosen, Fractal features of the digital measurement of length and area, Unpublished (1995).

[14] J. Wang, Y. Liu, P. Wei, Z. Tian, Y. Li, N. Zheng, Fractal image coding using SSIM, in: 2011 18th IEEE International Conference on Image Processing, IEEE, 2011, pp. 241–244.

[15] E. Zhao, D. Liu, Fractal image compression methods: A review, in: Third International Conference on Information Technology and Applications (ICITA'05), volume 1, IEEE, 2005, pp. 756–759.

[16] F. Berizzi, F. Dell'Acqua, P. Gamba, A. Garzelli, M. Martorella, On the fractal behavior of SAR images of ocean sea surface, in: IGARSS 2001. Scanning the Present and Resolving the Future. Proceedings. IEEE 2001 International Geoscience and Remote Sensing Symposium (Cat. No. 01CH37217), volume 4, IEEE, 2001, pp. 1729–1731.

[17] D. Chenoweth, B. Cooper, J. Selvage, Aerial image analysis using fractal-based models, in: 1995 IEEE Aerospace Applications Conference. Proceedings, volume 2, IEEE, 1995, pp. 277–285.

[18] N. Lam, Description and measurement of Landsat TM images using fractals, Photogrammetric Engineering and Remote Sensing 56 (1990) 187–195.

[19] L. Zhu, J. Yang, Fast multi-spectral image coding algorithm based on fractal, in: 2010 International Symposium on Intelligence Information Processing and Trusted Computing, IEEE, 2010, pp. 446–449.

[20] G. Di Martino, A. Iodice, D. Riccio, G. Ruello, I. Zinno, Fractal based filtering of SAR images, in: 2010 IEEE International Geoscience and Remote Sensing Symposium, IEEE, 2010, pp. 2984–2987.

[21] D. Riccio, G. Di Martino, A. Iodice, G. Ruello, I. Zinno, Fractal dimension images from sar images, in: 2014 IEEE International Conference on Image Processing (ICIP), IEEE, 2014, pp. 106–110.

[22] K. Sawada, S.-Y. Nagai, E. Nakamura, Fractal image coding combined with subband decomposition, in: ICECS 2001. 8th IEEE International Conference on Electronics, Circuits and Systems, volume 3, IEEE, 2001, pp. 1347–1350.

[23] Y. Xiu-hong, G. Bao-long, A novel non-local image inpainting algorithm: Fractal-based image inpainting, in: 2009 Second International Workshop on Computer Science and Engineering, volume 2, IEEE, 2009, pp. 26–30.

[24] Z. Bai, W. Zhang, M. Zhou, J. Bai, Algorithm designed for image inpainting based on decomposition and fractal, in: Proceedings of 2011 International Conference on Electronic & Mechanical Engineering and Information Technology, volume 3, IEEE, 2011, pp. 1552–1555.

[25] B. Dolez, N. Vincent, Sample selection in textured images, in: 2007 IEEE International Conference on Image Processing, volume 2, IEEE, 2007, pp. II–221.

[26] M. Ghazel, G. Freeman, E. Vrscay, Fractal image denoising, IEEE Transactions on Image Processing 12 (2003) 1560–1578.

[27] A. Malviya, Fractal based spatial domain techniques for image de-noising, in: 2008 International Conference on Audio, Language and Image Processing, IEEE, 2008, pp. 1511–1516.

[28] T. Hamano, K. Tokuda, M. Kaneko, Image restoration based on estimation of fractal structure, in: Proceedings of Digital Processing Applications (TENCON'96), volume 1, IEEE, 1996, pp. 311–316.

[29] I. Ismail, A. Hamdy, R. Frig, Studying the effect of down sampling and spatial interpolation on fractal image compression, in: The 2010 International Conference on Computer Engineering & Systems, IEEE, 2010, pp. 355–360.

[30] J. Jiang, Image compression with fractals, IEE Colloquium on Fractals in Signal and Image Processing, London, UK, (1995) 7/1–7/3.

[31] S. Nayak, A. Ranganath, J. Mishra, Analysing fractal dimension of color images, in: 2015 International Conference on Computational Intelligence and Networks, IEEE, 2015, pp. 156–159.

[32] Z. Shi, S. Yao, B. Li, Q. Cao, A novel image interpolation technique based on fractal theory, in: 2008 International Conference on Computer Science and Information Technology, IEEE, 2008, pp. 472–475.

[33] A.-Z. Shih, An examination of fractal dimension approach of image classification, in: 2008 International Conference on Machine Learning and Cybernetics, volume 6, IEEE, 2008, pp. 3156–3160.

[34] Y. Wee, H. Shin, A novel fast fractal super resolution technique, IEEE Transactions on Consumer Electronics 56 (2010) 1537–1541.

[35] S. Hong, D. Huidong, Fractal dimension applied in texture feature extraction in x-ray chest image retrieval, in: 2012 IEEE International Conference on Information and Automation, IEEE, 2012, pp. 841–845.

[36] E. Priya, S. Srinivasan, S. Ramakrishnan, Differentiation of digital TB images using multi-fractal analysis, in: 2011 24th Canadian Conference on Electrical and Computer Engineering (CCECE), IEEE, 2011, pp. 1431–1434.

[37] D. Qi, X. Jin, H. Wu, Application of multi-scale fractal feature in defects detection of log x-ray image, in: 2009 WRI Global Congress on Intelligent Systems, volume 3, IEEE, 2009, pp. 155–159.

[38] M. Tang, H. Wang, Feature analysis of brain MRI images based on fractal dimension, in: 2005 IEEE Engineering in Medicine and Biology 27th Annual Conference, IEEE, 2006, pp. 3245–3248.

[39] N. Avadhanam, S. Mitra, Analysis of texture images using robust fractal description, in: Proceedings of the IEEE Southwest Symposium on Image Analysis and Interpretation, IEEE, 1994, pp. 1–6.

[40] A. Costa, G. Humpire-Mamani, A. Traina, An efficient algorithm for fractal analysis of textures, in: 2012 25th SIBGRAPI Conference on Graphics, Patterns and Images, IEEE, 2012, pp. 39–46.

[41] P. Kumar, A wavelet based methodology for scale-space anisotropic analysis, Geophysical Research Letters 22 (1995).

[42] D. Po, M. Do, Directional multiscale modeling of images using the contourlet transfrom, IEEE Transactions on Image Processing 15 (2006) 1610 – 1620.

[43] J. Miya, A. Aghagotza, Edge detection using directional wavelet transform, in: Proceedings of the 12th IEEE Maditerranean Electrotechnical Conference, Dubronik, Canada, 2004.

[44] L. Zhang, J. Chen, B. Qiu, Region of interest extraction in remote sensing images by saliency analysis with normal directional lifting wavelet transform, Neurocomputing 179 (2016) 186–201.

[45] O. Nicolis, P. Raminez-Cabo, B. Vidakovic, 2D Wavelet based spectra with applications, Computational Statistics and Data Analysis 55 (2011) 738–751.

[46] S. Li, S. Dragicevic, F. Castro, M. Sester, S. Winter, A. Coltekin, C. Pettit, B. Jiang, J. Haworth, A. Stein, T. Cheng, Geospatial big data handling theory and methods: A review and research challenges, ISPRS Journal of Photogrammetry and Remote Sensing 115 (2016) 119–133.

[47] B. Mandelbrot, How long is the coast of Britain? statistical self-similarity and fractional dimension, Science 156 (1967) 636–638.

[48] B. Mandelbrot, The fractal geometry of nature, 1982. San Francisco, CA.

[49] B. Jiang, X. Liu, T. Jia, Scaling of geographic space as a universal rule for map generalization, Annals of the Association of American Geographers 103 (2013) 844–855.

[50] G. F. Jenks, Generalization in statistical mapping, Annals of the Association of American Geographers 53 (1963) 15–26.

[51] B. Jiang, J. Yin, Ht-index for quantifying the fractal or scaling structure of geographic features, Annals of the Association of American Geographers 104 (2014) 530–540.

[52] B. Jiang, Head/tail breaks: A new classification scheme for data with a heavy-tailed distribution, The Professional Geographer 65 (2013) 482–494.

[53] B. Jiang, Y. Miao, The evolution of natural cities from the perspective of location-based social media, The Professional Geographer 67 (2015) 295–306.

[54] T. Rajala, C. Redenbach, A. Särkkä, M. Sormani, A review on anisotropy analysis of spatial point patterns, Spatial Statistics 28 (2018) 141–168.

[55] J. Ratcliffe, Geocoding crime and a first estimate of a minimum acceptable hit rate, International Journal of Geographical Information Science 18 (2004) 61–72.

[56] R. Vatsavai, V. Chandola, S. Klasky, A. Ganguly, A. Stefanidis, S. Shekhar, Spatiotemporal data mining in the era of big spatial data: algorithms and applications, in: ACM Conference SigSpatial Big Spatial, 2012.

[57] S. Shekhar, M. Evans, J. Kang, P. Mohan, Identifying patterns in spatial information: a survey of methods, Wiley Interdisciplinary Reviews: Data Mining and Knowledge Discovery 1 (2011) 193–214.

[58] H. Miller, M. Goodchild, Data driven geography, GeoJournal 80 (2015) 449–461.

[59] M. Evans, D. Oliver, X. Zhou, S. Shekhar, Big Data: Techniques and Technologies in Geoinformatics, CRC Press, 2014.

[60] M. Evans, D. Oliver, K. Yang, X. Zhou, R. Ali, S. Shekhar, Cyber GIS for Geospatial Discovery and Innovation, Springer, Dortrecht, 2018, pp. 143–170.

[61] Z. Shekhar, S. Jiang, Spatial Big Data Science, Springer, 2017.

[62] D. Cugler, D. Oliver, M. Evans, S. Shekhar, C. Medeiros, Spatial big data: platforms, analytics, and science., GeoJournal (2013).

[63] M. Goodchild, The quality of big(geo)data, Dialogues in Human Geography 3 (2013).

[64] D. Lopez, N. Gunasekaran, B. Murugan, H. Kaur, K. Abbas, Spatial big data analytics of Influenza epidemic in Vellore, India, in: 2014 IEEE Conference on Big Data, 2014, pp. 19–24.

[65] J. Yu, J. Wu, M. Sarwat, A demonstration of geospark: A cluster computing framework for processing big spatial data, ICDE 2016 IEEE Conference (2016).

[66] X. Chen, H. Vo, A. Aji, F. Wang, High performance integrated spatial big data analytics, in: 3rd ACM Sigspatial International Workshop on Analytics for Big Geospatial Data, 2014, pp. 11–14.

[67] C. Jardak, P. Mahonen, J. Riihijarvi, Spatial big data and wireless networks: experiences, applications, and research challenges, IEEE Network (2014) 26–31.

[68] X. Li, W. Li, L. Anselin, S. Rey, J. Koschinsky, A mapReduce algorithm to create contiguity weights for spatial analysis of big data, in: Proceedings of the 3rd ACM SIGSPATIAL International Workshop on Analytics for Big Geospatial Data, 2014, pp. 50 – 53.

[69] G. Manogaran, D. Lopez, Spatial cumulative sum algorithm with big data analytics for climate change detection, Computers and Electrical Engineering 65 (2018) 207–221.

[70] G. Zhang, A.-X. Zhu, Q. Huang, A GPU-accelerated adaptive kernel density estimation approach for efficient point pattern analysis on spatial big data, International Journal of Geographical Information Science 31 (2017) 2068–2097.

[71] G. Zhang, Q. Huang, A.-X. Zhu, J. Heel, Enabling point pattern analysis on spatial big data using cloud computing: optimising and accelrating Ripley's K-function, International Journal of Geographical Information Science 30 (2016) 2230–2252.

[72] S. Wang, Y. Zhang, H. Lu, E. Wang, W. Yun, W. Cai, Geospatial big data analytics engine for spark, in: ACM Conference SigSpatial Big Spatial, 2017.

[73] R. Anguelov, I. Fabris-Rotelli, LULU operators and discrete pulse transform for multidimensional arrays, IEEE Transactions on Image Processing 19 (2010) 3012–3023.

[74] J. Illian, A. Penttinen, H. Stoyan, D. Stoyan, Statistical analysis and modelling of spatial point patterns, volume 70, John Wiley & Sons, 2008.

[75] D. König, V. Schmidt, Directional distributions for multi-dimensional random point processes, Stochastic Models 8 (1992) 617–636.

[76] M. Rosenberg, Wavelet analysis for detecting anisotropy in point patterns, Journal of Vegetation Science 15 (2004) 277–284.

[77] O. Nicolis, J. Mateu, R. D'Ercole, Testing for anisotropy in spatial point processes, in: Proc 5th Int Workshop on Spatio-Temporal Modelling (METMA5). Gonzalez-Manteiga et al.(Eds.), Publisher Unidixital. ISBN, 2010, pp. 978–840934272.

[78] J. Ohser, D. Stoyan, On the second-order and orientation analysis of planar stationary point processes, Biometrical Journal 23 (1981) 523–533.

[79] D. Stoyan, V. Beneš, Anisotropy analysis for particle systems, Journal of Microscopy 164 (1991) 159–168.

[80] T. Rajala, A. Särkkä, C. Redenbach, M. Sormani, Estimating geometric anisotropy in spatial point patterns, Spatial Statistics 15 (2016) 100–114.

[81] Y. Guan, M. Sherman, J. Calvin, Assessing isotropy for spatial point processes, Biometrics 62 (2006) 119–125.

[82] M. de Lancey, I. Fabris-Rotelli, Effective graph sampling of a nonlinear image transform, in: Proceedings of FAIR 2019, volume 2540,, Cape Town, 2019, pp. 185 – 195,. Http://ceur-ws.org/Vol-2540/.

[83] I. Fabris-Rotelli, G. Stoltz, On the leakage problem with the discrete pulse transform decomposition, in: Proceedings of the 23rd Annual Symposium of the Pattern Recognition Association of South Africa, 2012, pp. 179–186. A de Waal (Ed.), ISBN: 978-0-620-54601-0.

[84] B. Jiang, Wholeness as a hierarchical graph to capture the nature of space, International Journal of Geographical Information Science 29 (2015) 1632–1648.

[85] A. Hyvärinen, J. Hurri, P. Hoyer, Natural Image Statistics: A Probabilistic Approach to Early Computational Vision, Springer Science and Business Media, 2009.

[86] P. Gao, Z. Liu, M. Xie, K. Tian, G. Liu, CRG index: A more sensitive ht-index for enabling dynamic views of geographic features, The Professional Geographer 68 (2016) 533–545.

[87] P. Gao, Z. Liu, K. Tian, G. Liu, Characterizing traffic conditions from the perspective of spatial-temporal heterogeneity, ISPRS International Journal of Geo-Information 5 (2016) 34.

[88] L. Anselin, What is Special About Spatial Data? Alternative Perspectives on Spatial Data Analysis (89-4), Technical Report, National Center for Geographic Information and Analysis, Santa Barbara, CA, 1989.

[89] M. Goodchild, Giscience, geography, form, and process, Annals of the Association of American Geographers 94 (2004) 709–714.

[90] D. Ma, M. Sandberg, B. Jiang, Characterizing the heterogeneity of the openstreetmap data and community, ISPRS International Journal of Geo-Information 4 (2015) 535–550.

[91] B. Jiang, Geospatial analysis requires a different way of thinking: The problem of spatial heterogeneity, GeoJournal 80 (2015) 1–13.

[92] F. Richard, Tests of isotropy for rough texturesof trended images, Statistica Sinica 26 (2016) 1279–1304.